PHILOSOPHICAL TRANSACTIONS OF THE ROYAL SOCIETY A MATHEMATICAL, PHYSICAL & ENGINEERING SCIENCES

Molecular dynamics in intense laser fields

The Royal Society

Phil. Trans. R. Soc. Lond. A 1999 **357**, 1309-1329
doi: 10.1098/rsta.1999.0376

THE ROYAL SOCIETY

Molecular dynamics in intense laser fields

By Jim F. McCann[1]† and Jan H. Posthumus[2]

[1]*Physics Department, University of Durham, Durham DH1 3LE, UK*
[2]*J. J. Thomson Physical Laboratory, University of Reading, Whiteknights, Reading RG6 6AF, UK*

We discuss recent developments in the study of the interaction of intense lasers with diatomic molecules. An overview of theory and experiment is given and particular attention is given to the energy spectra of ions resulting from photodissociative ionization. The ionization process is studied in the multiphoton regime using Floquet theory and compared with field-ionization results appropriate for the tunnelling regime. A review is given of the evidence for the existence of *critical distances* between the nuclei at which ionization rates are strongly enhanced. The field-ionization model is found to reproduce the main features observed by experiments. The field-ionization Coulomb explosion (FICE) model accurately reproduces the kinetic energy releases and threshold intensities of the various fragmentation channels of the iodine dimer: I_2. With the three-dimensional FICE model, threshold intensities as a function of angle between the molecular axis and the laser E-field are calculated. The angular distributions obtained are in good agreement with measurements taken for distributions of I_2 fragments. The angular distributions of the H_2 and N_2 fragments, on the other hand, are much more sharply peaked, indicating reorientation by the laser field.

Keywords: multiphoton processes; Coulomb explosion; dissociative ionization; molecular dynamics; intense lasers

1. Introduction

The crucial role of the photoelectric effect in the historical development of the quantum theory is well documented. While rudimentary physics textbooks point out that no photoelectrons are created if the quantum of light energy falls below the work function/ionization potential of the target material, if the light source is intense then a significant photoelectron yield can be obtained through multiple photoabsorption. In fact, at the highest intensities it is possible to ionize completely any atoms or molecules in the path of such light. In this article, we discuss the physics of the interaction of such highly intense lasers with simple homonuclear diatomic molecules.

The primary influence of an intense laser is to subject the bound electrons to an electromagnetic tug-of-war between the external and internal forces. At high intensities, by this we mean values for which the peak electric field of the laser is comparable to the electrostatic internal fields, electrons can be readily stripped from their parent molecules even in the absence of intermediate resonant states. Consequently, the shielding and bonding effect of the electrons is lost and the molecule disintegrates.

† Present address: Department of Applied Mathematics and Theoretical Physics, The Queen's University of Belfast, Belfast BT7 1NN, UK.

For example, although ionization of the helium atom with a Ti:sapphire laser ($\lambda \approx 780$ nm) requires at least 16 photons, at an intensity of 10^{15} W cm^{-2}, the ionization probability nevertheless approaches 100% in *ca.* 100 fs (Walker *et al.* 1994). Furthermore, there is a significant probability of double ionization, a process that requires at least an extra 34 photons. It is no surprise then, that such strong and fast interactions cannot be described by perturbation theory. A detailed discussion of intense-laser interactions with the helium atom is described in an accompanying paper (Taylor & Dundas, this issue). What may come as a surprise, however, is the fact that many of the distinct intense-laser phenomena can be understood, qualitatively and quantitatively, in quite simple terms. Illustrative of this is the *simpleman's* model for above threshold ionization (ATI), where excess photons are absorbed on top of the minimum amount required (van Linden van den Heuvel & Muller 1988).

Molecules not only ionize in intense laser fields, but dissociate as well. For low-intensity light, photodissocation is the most likely fragmentation process. However, as the light intensity increases then ionization becomes a significant process, and one observes photodissociative ionization producing a large variety of ionic fragments (Codling & Frasinski 1993). The partitioning of photon energy among the ionic and electronic fragments is determined by factors such as pulse shape, bandwidth and peak intensity. In addition to these variables, we have intensity and density variations over the focal volume. The variations in these parameters give rise to a wide variety of phenomena, some of which can be exploited in applications such as high-order harmonic generation, isotope separation, and plasma heating. However, this complexity can also lead to difficulties in the analysis of these effects. While this subject is an active area of current investigation, it is fair to say that the detailed explanation of these processes is far from being understood at this time. One aspect of the problem that is reasonably well understood concerns the energy distributions of ionic fragments. On the other hand, considerably less is known about the absolute yields and relative populations of the ionic states, and the electron spectra have yet to be studied with quite the same degree of precision. Moreover, the study of polyatomics (Sanderson *et al.* 1998) and clusters (Shao *et al.* 1996) has produced some startling results. Clearly, this is an ongoing and active area of current research and much remains to be done.

The problem is inherently difficult, for experimentalists and theorists, owing to the proliferation of many-body continuum channels. So far laboratory studies have concentrated on simple diatomic systems through the observation of fragment ions using techniques such as covariance mapping (Codling & Frasinski 1993). While theory has been less well developed, nonetheless one can make some progress with the interpretation of such data for systems as complex as SF_6 (Sanderson *et al.* 1997) with simplified models which treat the ionization process as a sequence of electron release processes, and neglect the multielectron interactions. It has become clear recently that a semiempirical model based on such ideas, the field-ionization Coulomb explosion (FICE) theory, can account for a great deal of the data observed to date. We discuss this model in detail below.

2. Photoionization

The physical character of intense-laser ionization of molecules is loosely divided into two types. Firstly, *tunnelling ionization* in which the laser acts as a strong quasi-

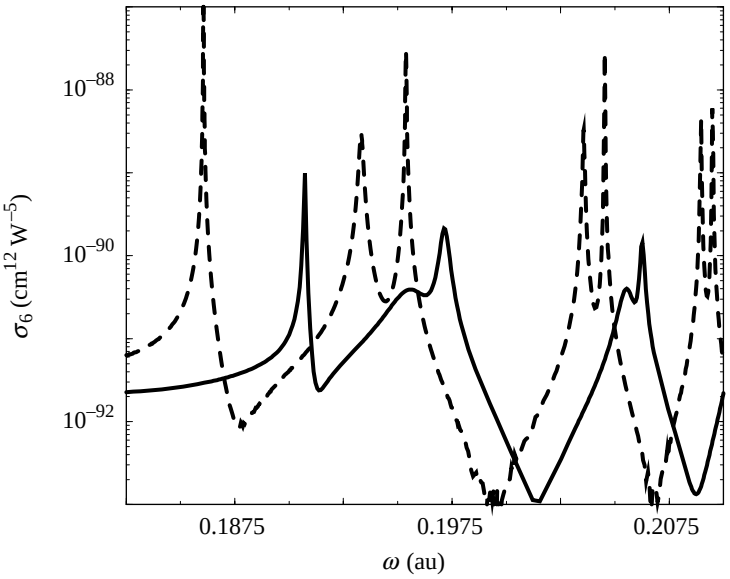

Figure 1. Resonance-enhanced multiphoton ionization in H_2^+. Generalized cross-sections (σ_6) for six-photon ionization of H_2^+ at equilibrium separation ($R = 2a_0$). The graphs show the non-perturbative behaviour of resonance positions and widths arising from strong molecule–field coupling. Data for three intensities are presented as an illustration of this behaviour. The lowest intensity corresponds to leading-order perturbation approximation: - - - -, 5×10^{12} W cm^{-2}; ———, 5×10^{13} W cm^{-2}.

static electric field that allows the electrons to escape from the parent atom by a tunnelling (field-ionization) process. Secondly, *multiphoton ionization* in which the electron acquires energy by climbing a ladder of electronic states to reach the continuum through multiphoton absorption. The classification is guided by the value of the Keldysh parameter, γ, which is a measure of the ratio of *tunnelling time* to the *optical period*, T (Keldysh 1965). Thus γ is proportional to the laser frequency and inversely proportional to the laser field strength, so that $\gamma \ll 1$ corresponds to *tunnelling ionization* produced by a low-frequency intense laser. The converse conditions ($\gamma \gg 1$) correspond to *multiphoton ionization* in which an electron, though inhibited from tunnelling out of the atom, can gain energy from the field through the combination of the harmonic external force and the anharmonic internal force. The electron thus gathers several quanta (or harmonics) of energy from the field and is able to overcome the binding force.

Equivalently, γ is a measure of the relative size of the binding energy of the electron ($|E_0|$) to the kinetic (ponderomotive) energy of a free-electron in the laser field $U_\mathrm{p} = (F/2\omega)^2$, where F is the amplitude of the electric field intensity due to the laser, and ω is the angular frequency of the light, all quantities being expressed in atomic units. Thus we have the definition: $\gamma = (|E_0|/2U_\mathrm{p})^{1/2}$. The distinction between a *tunnelling* and *multiphoton* process is useful from a conceptual and practical viewpoint. One can use this criterion to help interpret the experimental data and to establish a suitable method for calculations.

In the following sections, we will describe some commonly used methods for

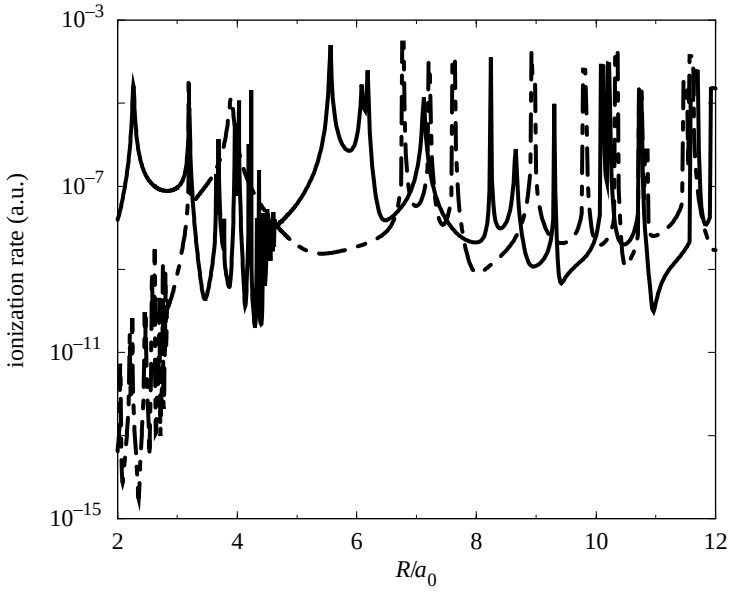

Figure 2. The resonance structure of the ionization rate as functions of bond length (R). The wavelength and intensity are fixed at $\lambda = 248$ nm and $I = 5 \times 10^{12}$ W cm^{-2}. Results for the two lowest dressed states are shown; the avoided crossing occurs at $R = 3.2a_0$: ———, upper state; - - - -, lower state.

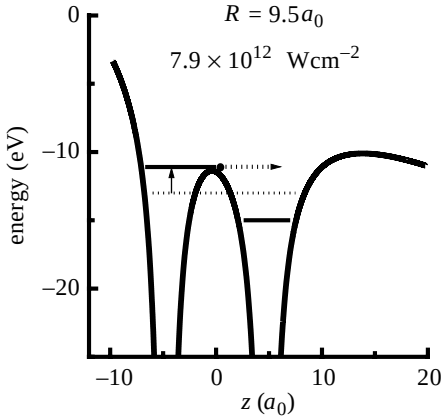

Figure 3. One-dimensional representation of the potential well for a valence electron inside a diatomic molecule and subjected to an external electric field. In the field-ionization, Coulomb explosion model the the central potential barrier impedes the adiabatic adjustment of the molecule to the laser field.

describing dissociative ionization of molecules: (*a*) the Floquet method; (*b*) the quasi-static field method; (*c*) the wave packet method; and (*d*) the field-ionization Coulomb explosion model. Detailed quantum mechanical results for the hydrogen molecular ion H_2^+ are discussed and then compared with experimental findings. We focus on very recent developments in this field, but for a very perceptive and comprehensive review of theory and experiment for the interactions of intense light with molecular

hydrogen, we refer the reader to the articles of Giusti-Suzor *et al*. (1995) and Codling & Frasinski (1993).

(*a*) *Floquet theory*

If the laser pulse duration (T_{D}) is sufficiently long, so that the electric field can be represented as a monochromatic field with slow amplitude modulation, then, to a good approximation, the external field represents a sinusoidal perturbation of the system. For systems under the influence of time-dependent periodic potentials, the Fourier decomposition of the wave function reduces the problem to the solution of an infinite set of time-independent equations.

The Floquet method has been applied extensively in recent years to the interaction of intense light with atoms and molecules. We will not attempt to describe the method in detail, but simply outline some salient features and refer the reader to Potvliege & Shakeshaft (1992) for an extensive discussion. For simplicity, let us assume a one-electron diatomic molecule with fixed nuclei. Thus if $V(\boldsymbol{r}, t+T) = V(\boldsymbol{r}, t)$ then a solution of the time-dependent Schrödinger equation,

$$[H(\boldsymbol{r}, \boldsymbol{p}) + V(\boldsymbol{r}, t)]\Psi(\boldsymbol{r}, t) = \mathrm{i}\hbar \frac{\partial}{\partial t}\Psi(\boldsymbol{r}, t), \tag{2.1}$$

is given by

$$\Psi_j(\boldsymbol{r}, t) = \mathrm{e}^{-\mathrm{i}\varepsilon_j t/\hbar} \sum_{N=-\infty}^{+\infty} \mathrm{e}^{-\mathrm{i}N\omega t}\Phi(j, N; \boldsymbol{r}), \tag{2.2}$$

with $\omega = 2\pi/T$. This equation defines the quasi-energy ε_j, and the Floquet wave function (or 'dressed state' function) $\Phi(j, N; \boldsymbol{r})$. Clearly, the quasi-energy is indeterminate to within multiples of the fundamental frequency ω. Thus ε_j is equivalent, in physical terms, to the sequence of harmonics: $\varepsilon_j \pm \hbar\omega, \pm 2\hbar\omega, \ldots$. In addition, as the system is open to fragmentation, this quasi-energy is complex and its imaginary part represents the decay rate of the bound states. In order to determine ionization rates, we require the quasi-energy.

In practice, this harmonic expansion is truncated for numerical stability and to accommodate the resources of the computer; thus $N_{\min} \leqslant N \leqslant N_{\max}$. As a result the periodicity of the quasi-energy ($\varepsilon_j, \varepsilon_j \pm \hbar\omega, \ldots$) is disturbed. As one might expect, the deviations are most pronounced at the upper and lower ends of the energy spectrum, where the effect of truncation is most noticeable. In practice, this periodicity provides a very useful test of the convergence of the numerical results with respect to the number of Floquet harmonics ($N_{\max} + 1 - N_{\min}$). Thus it is possible to test the reliability of results for the quasi-energy by observing whether the eigenvalue periodicity is well satisfied, and whether the results are sensitive to an increase in the number of Floquet harmonics.

Making use of the Floquet ansatz (equation (2.2)) and taking the potential to have the sinusoidal form,

$$V(\boldsymbol{r}, t) = V_- \mathrm{e}^{\mathrm{i}\omega t} + V_+ \mathrm{e}^{-\mathrm{i}\omega t}, \tag{2.3}$$

the time-dependent Schrödinger equation is reduced to an infinite set of time-independent differential equations coupling next-neighbour Fourier components:

$$(\varepsilon_j + N\hbar\omega - H)|\Phi(j, N)\rangle = V_+|\Phi(j, N-1)\rangle + V_-|\Phi(j, N+1)\rangle. \tag{2.4}$$

Physically, the action of the operator V_- corresponds to single-photon emission and conversely, that of V_+ corresponds to absorption. The molecule–field interaction operator $V_\pm$ can be expressed in the length or velocity gauges. There is no physical distinction between the use of either gauge for the calculation of the properties of a system interacting with light. Indeed this equivalence provides an important method for checking the accuracy of the results obtained. Finally, we represent the state *kets* in terms of basis functions and apply physical boundary conditions corresponding to outgoing photoelectrons (details are given in Plummer & McCann (1995*a*, *b*)). This leads to a generalized eigenvalue problem which can be solved by standard methods to yield the required quasi-energies.

Returning to our model system, consider a hydrogen molecular ion at equilibrium separation ($R = 2a_0$). Furthermore, we will restrict our attention to *parallel* transitions. This is equivalent to assuming the molecular axis is aligned along the direction of linear polarization of the light. Figure 1 shows generalized cross-sections for a range of frequencies for which a minimum of six photons are required to ionize the molecule from the ground state. For a multiphoton process in which a minimum of M photons are required to ionize the molecule, it is useful to define a *generalized* cross-section in terms of the ionization rate and laser intensity:

$$\sigma_M = \hbar\omega\Gamma/(I^M). \tag{2.5}$$

For a low-intensity M-photon ionization process, leading-order perturbation theory predicts the result $\Gamma \propto I^M$, in which case σ_M is independent of intensity. Thus, variations of σ_M with intensity indicate non-perturbative behaviour as may be seen in figure 1. The generalized cross-sections show a variation in the width and position of the resonances. The displacements in energy are termed AC Stark shifts, and are due to virtual absorption–re-emission processes. For example, the resonance located at $\omega \approx 0.186$ au for an intensity of $I = 5\times10^{12}$ W cm^{-2} moves to $\omega \approx 0.195$ au as the intensity is increased to 10^{14} W cm^{-2}. This particular resonance may be identified with an ionization channel going through a four-photon transition to a higher lying electronic state (Baik *et al.* 1996). All other lines in figure 1 correspond to five-photon resonance transitions. In the notation used to describe resonant enhanced multiphoton ionization (REMPI) an $M + N$ photon resonance denotes the fact that M-photon absorption leads to a resonance and additional N photons to ionization. Thus the peaks may all be identified as $4 + 2$ and $5 + 1$ REMPI resonances. The asymmetric non-Lorentzian shapes of the five- and four-photon resonances in figure 1 are familiar from very early studies in atomic multiphoton ionization (Maquet *et al.* 1983). The modification of the resonance structure due to laser power is also seen in terms of the broadening and merging of some peaks. These results are an illustration of the sensitivity of ionization rate to the presence of resonances, and also the large effects that strong laser power can have on the positions and widths of resonances.

Consider the molecular ion in vibrational motion induced by the light source. In this case, a change in R implies a change in the electronic energy level structure. Therefore, the REMPI structure will differ at each R. Thus for a fixed frequency of light we will observe a sequence of resonance features as R changes. Instead of scanning the laser frequency, as in figure 1, the molecular expansion scans the energy spectrum. The determination of the ionization rate as a function of R is critical in determining the resulting ion kinetic energies.

In particular, as the molecule dissociates, the binding energy of the electronic orbital is reduced, and lower numbers of photons are required to ionize the molecule.

This behaviour is illustrated in figure 2, which presents the resonance structure of the ionization rate as functions of bond length (R). The wavelength and intensity are fixed at $\lambda = 248$ nm and $I = 5 \times 10^{12}$ W cm^{-2}. Results for the two lowest dressed states are shown; the avoided crossing occurs at $R = 3.2a_0$ and details are given in Madsen & Plummer (1998). With reference to figure 2, for large bond lengths ($R \geqslant 5a_0$), where four photons are required to ionize the ground-state molecular ion, the full curve in figure 2 is characterized by a series of well-separated resonances, which may all be identified as $3 + 1$ resonances, except the lower structure in the double peak situated at $R \approx 6a_0$, which is a $2 + 2$ resonance. The inner region ($R \leqslant 5a_0$) is characterized by two Rydberg series, the first passing through the five-photon ionization threshold just below $R = 3a_0$ and the second passing through the four-photon threshold at $R \approx 4.8a_0$. The resonances in the first Rydberg series all arise from five-photon excitations, whereas the resonances in the latter originate from four-photon transitions. In practical terms it is impossible to represent the full (infinite) Rydberg series near threshold as one is limited by the type of basis function and the size of the function set.

These data allow us to identify *critical distances*, values of R for which ionization is strongly enhanced, for dissociative ionization. For example, a vibrating/dissociating molecule will expand from equilibrium bond length passing through these resonances in turn. Any large ionization peaks will then lead to ions having a Coulomb energy appropriate to this bond length. Clearly, observation of the ejected ion energy spectrum will contain a signature of such a pattern. Although the sharp resonance structure will inevitably be broadened or suppressed by the motion of the nuclear wave packet, there will be sensitivity to the mass (isotope) of the ejected nucleus.

(*b*) *Quasi-static field ionization*

If the laser frequency is much lower than the orbital frequency of the electron, the laser interaction can be treated as a quasi-static external electric field. One can allow for the sinusoidal oscillations by time-averaging this static field (Plummer & McCann 1996). This can be shown to reproduce qualitatively time-dependent wave packet results (Plummer & McCann 1995*a*, *b*; Zuo & Bandrauk 1995). A representation of the potential energy well for the electron in H_2^+ and in the presence of an external (DC) field aligned along the molecular axis illustrates this point (figure 3). Estimating the ionization rate for this time-independent problem is straightforward.

A detailed calculation of the ionization of this state is presented in figure 4. It is clear that there are resonance structures according to the bond length of the molecular ion. These resonances can be qualitatively explained in terms of the potential barrier heights (figure 3). This forms the basis of the classical FICE model that we discuss later. The resonance features are evidence that, as in the case of *multiphoton ionization*, for a given field strength, certain bond lengths give rise to *critical distances* at which ionization is strongly enhanced. A detailed study of these features is given by Plummer & McCann (1997), but let us briefly summarize the main conclusions. The absolute values of the ionization rates are highly sensitive to field strength, for example doubling the field amplitude can increase the ionization rate by two orders of magnitude. Thus ionization, if it occurs, takes place predominantly at the peak intensities of the laser field cycle. Next, for increasing field strengths, the critical distances contract and the inner peak increases in importance. Regarding the

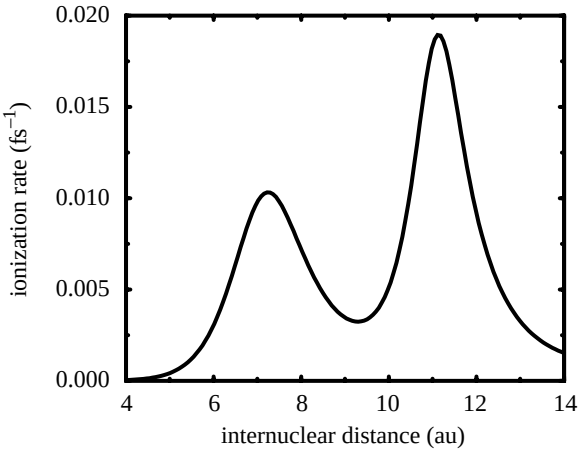

Figure 4. Static field ionization rate variation with internuclear distance. Data for the H_2^+ ion (upper electronic state), with field strength $F = 0.04$ au.

orientation of the molecular ion with respect to the field and for low laser intensities, the ionization yields are much higher when the molecular axis is aligned with the field. However, for very high field strengths the ionization rates are much less sensitive to molecular orientation. We shall see that this is supported by experimental evidence regarding the angular distribution of fragment ions.

(*c*) *Short-pulse coherent photodissociative ionization*

The use of ultrashort laser pulses to probe the time domain of dissociation processes is a well-established technique. Since molecular vibrations and dissociation occur on subpicosecond time-scales, the availability of pulses of the duration 10–100 fs has made it possible to probe the photodissociative ionization process for heavy molecules. Fragment atoms such as hydrogen and lithium, and their isotopes, are more difficult to study in this way; because of their small mass, they dissociate very rapidly. A complementary technique is to extend the pump-probe method, widely used as a probe in the reciprocal space (energy/frequency), to investigate such systems. Very recently, these techniques have been combined in an experimental study of photodissociative ionization of H_2 using coherent ultrashort laser pulses (Thompson *et al*. 1997).

The coherence between two-colour ultrashort pulses can only be studied using direct time-dependent (wave packet) methods. For simplicity, let us assume that the lasers have a common axis of linear polarization, then the effective electric field of the light will be of the form,

$$F(t) = F_{01}(t)\cos(\omega_1 t) + F_{02}(t)\cos(\omega_2 t + \phi), \tag{2.6}$$

in which $\omega_{1,2} = 2\pi c/\lambda_{1,2}$ and the pulse envelopes are described by the factors: $F_{01,02}(t)$. We denote the phase difference as ϕ. Let us consider the polarization of the light to be along the molecular axis and that the pulse duration (T_D) is short enough to neglect rotational motion. It is possible to solve the Schrödinger equation for the electronic motion (in three dimensions) and the nuclear motion (in one dimension) without any difficulty. The method we adopt is based on a three-dimensional basis

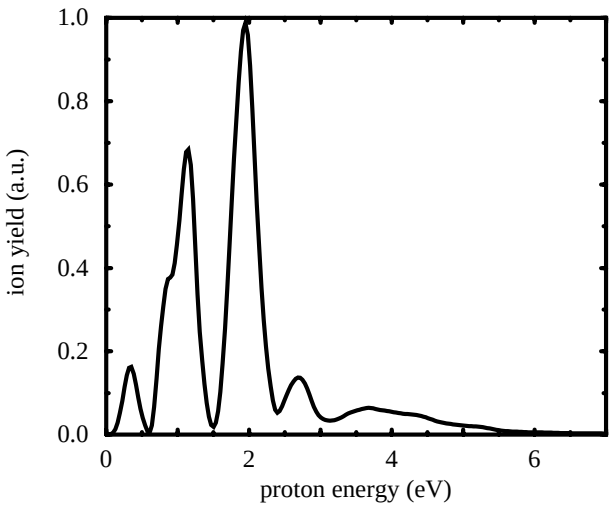

Figure 5. Proton spectrum for a 20 fs two-colour pulse: $\lambda_1 = 750$ nm, $\lambda_2 = 375$ nm; phase difference, $\phi = 0$. This spectrum shows the dissociative ionization peaks as well as a small Coulomb explosion peak near 4 eV, in agreement with the quasi-static field model.

function expansion for the electron(s) combined with a discretization of the nuclear vibrational wave function on a one-dimensional grid of points.

The coherence/interference effects will be strongest when the field strengths are of comparable size. In figure 5 we show sample results for proton energy spectra for a $T_D = 20$ fs pulse with a peak intensity of $I = 0.56 \times 10^{14}$ W cm^{-2}. The pulse profile is given by (in atomic units) $F_{01} = F_{02} = 0.04 \sin^2(\pi t/T_D)$, and we take $\phi = 0$. Referring to figure 5, one can clearly see a sequence of proton energy peaks corresponding to dissociative ionization channels. The peaks are assigned as follows, in increasing energy:

$$(\omega_2, 2\omega_1) \qquad (\omega_2 + \omega_1, 3\omega_1) \qquad (2\omega_2, \omega_2 + 2\omega_1, 4\omega_1) \qquad (2\omega_2 + \omega_1, \omega_2 + 3\omega_1, 5\omega_1).$$

The broad peak around 4 eV corresponds to Coulomb explosion. This is in agreement with the quasi-static field results of Plummer & McCann (1997), which predict a value of R_c of 3.4 au for $F = 0.08$. The interest in such processes is that, by variation of phase difference and relative field strengths, one can exercise a measure of coherent control over the process.

Given the success of the quasi-static result, and the fact that it is rather simple to program, it is convenient to use these data to compare with experiment. Thompson *et al.* (1997) performed such a test, and the results of their simulations are shown in figures 6 and 7. Figure 6 shows a log–log plot of total ion signals of the various ion channels versus the laser intensity when H_2 is subjected to pulses of 85 fs in duration and at a wavelength of 375 nm. These results were simulated, assuming that the processes of ionization, dissociation and Coulomb explosion are sequential, by solving the coupled differential equations for the transition rates and including the influence of the intensity distribution in the laser focus. The best fit to the data (solid curves in figure 6) was obtained with population probabilities as shown in figure 7*a*. The probabilities are given as a function of the local laser intensity in the focus. The corresponding rates for the various transitions are shown in figure 7*b*. Although this

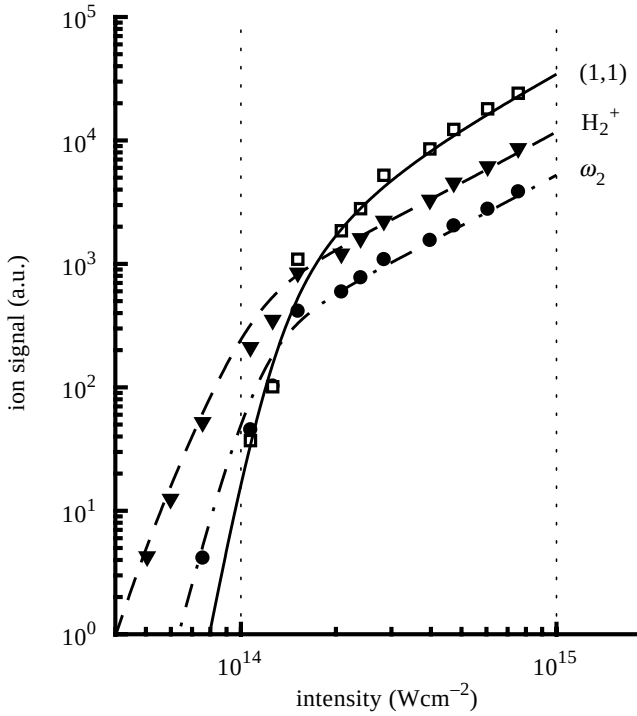

Figure 6. Log–log plot of the ion signal versus laser intensity for H_2 subjected to an 85 fs pulse at $\lambda = 375$ nm. The smooth curves are based on theory simulations described in the text, the symbols represent the experimental data.

modelling involved some significant simplifying assumptions, the agreement of the (1,1) rates with theoretical values from Plummer & McCann (1996) is remarkably good.

3. A classical approach to heavy diatomic molecules

(*a*) *A simple model for field-ionization and Coulomb explosion*

When diatomic molecules such as N_2 and I_2 are subjected to intense laser pulses, fragment ions are observed with kinetic energies that are typically about half of the values one would obtain from Coulomb explosion at the equilibrium internuclear distance of the neutral molecule (Codling & Frasinski 1993). It has become clear recently that these characteristic kinetic energies can be associated with the enhancement of the ionization probabilities at the critical internuclear separation, R_c (Posthumus *et al*. 1995; Seideman *et al*. 1995; Zuo & Bandrauk 1995; Chelkowski *et al*. 1995; Kulander *et al*. 1996; Posthumus *et al*. 1996*a*, *b*). When a molecule dissociates through the influence of a laser, the central potential barrier, separating the two ionic cores, obviously rises. At R_c, this barrier has risen to such an extent that it inhibits the adiabatic adjustment of the molecule to the laser E-field (figure 3). Thus the molecule makes diabatic transitions to excited states with the result that the probability of field ionization is enhanced. A classical FICE model has been developed (Posthumus *et al*. 1996*a*, *b*) in order to describe the dissociative ionization

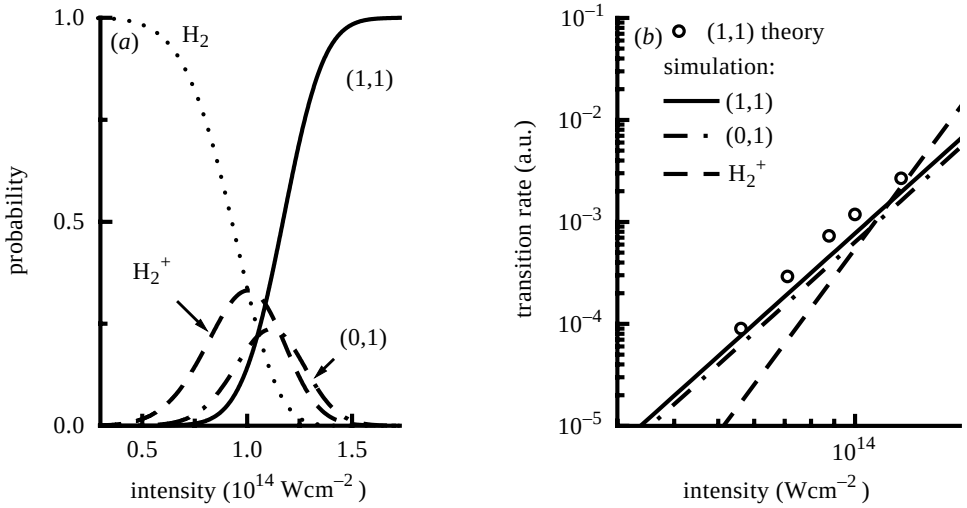

Figure 7. (*a*) Population probabilities that lead to the simulation shown in figure 6 at 375 nm. (*b*) Simple power-law transition rates, which were adjusted to yield the curve fits of figure 6. Also shown are the field ionization theory data from Plummer & McCann (1996).

process in simple terms. The FICE model allows us to calculate the minimum laser intensities that are required for over-the-barrier ionization as a function of internuclear separation. For example, consider the following one-dimensional model of a molecular ion. The double-well potential, $U(x)$, in which the outer electron moves is modelled by (Posthumus *et al.* 1996*a*)

$$U(x) = -\frac{\frac{1}{2}Q}{|x+\frac{1}{2}R|} - \frac{\frac{1}{2}Q}{|x-\frac{1}{2}R|} - \mathcal{E}x, \tag{3.1}$$

where $Q = Q_1 + Q_2$ is the sum of the ionic core charges, x is the axial coordinate of the electron, R is the internuclear separation and $\mathcal{E}$ is the laser E-field (atomic units are used throughout). The energy level, E_{L} , of the outer electron in this symmetric, double well is approximated by

$$E_{\mathrm{L}} = \tfrac{1}{2}(-E_1 - Q_2/R) + \tfrac{1}{2}(-E_2 - Q_1/R), \tag{3.2}$$

where E_1 and E_2 are the known ionization potentials of the atomic ions. The complex adiabatic excitation at R_{c} is modelled by a Stark shift that is only present when the unperturbed level is below the central barrier; see figure 3. Even then one assumes that the Stark shift only operates up to the point of delocalization, i.e. to the top of the central barrier. The maximum excitation is therefore equal to

$$\Delta E_{\max} = \tfrac{1}{2}\mathcal{E}R. \tag{3.3}$$

Appearance intensities for fragmentation channels (Q_1, Q_2) are found from the minimum E-field that lowers the outer potential barrier below the (raised) electron energy level. In figure 8 we present such appearance intensities for I_2 (full curves). With the form of equation (3.1) we have assumed that the double potential wells are symmetric. However, for large values of R, where the two ion cores are well separated, this assumption is invalid for asymmetric channels such as (1, 2). This channel must be as difficult to create as the (2, 2) channel, because both involve

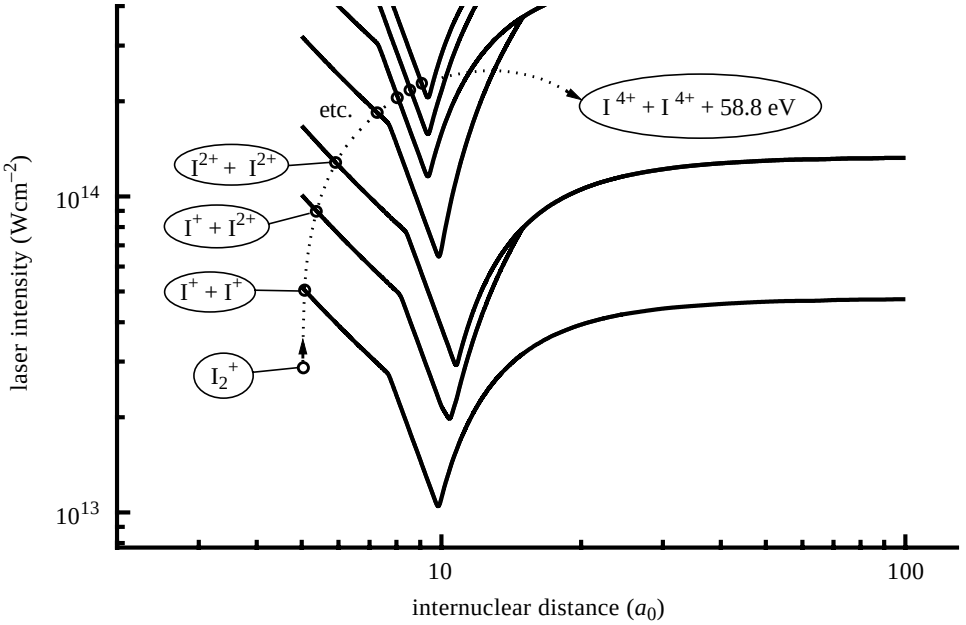

Figure 8. Appearance intensities for the various fragmentation channels of I_2 (full curves). The broken curve traces the evolution of R versus laser intensity for 150 fs pulses at an intensity of 2.5×10^{14} W cm^{-2}. Note that all appearance intensities have a minimum close to $R = 10a_0$, the critical internuclear distance for iodine.

the appearance of an effectively free I^{2+} ion. The curves of the asymmetric channels are therefore allowed to approach the curves of the next higher symmetric channels between R_c and $R = 15a_0$ (see figure 8). It is clear from figure 8 that the critical internuclear separation, R_c, is virtually identical for all channels. This is because the enhanced ionization process is so closely related to electron localization, which starts at roughly the same separation for all channels (Posthumus *et al.* 1995).

(*b*) *Classical trajectory calculations*

Fragment kinetic energies can be estimated from the equation $E = Q_1Q_2/R_c$, since ionization occurs mainly around R_c and the kinetic energy release is dominated by Coulomb repulsion. More accurate results are obtained with classical trajectory calculations. As an example, let us calculate such a trajectory for an I_2 molecule subjected to a laser pulse of duration 150 fs and peak intensity 2.5×10^{14} W cm^{-2}. The molecule is ionized and starts to dissociate slowly on the leading edge of the pulse at an intensity of approximately 3×10^{13} W cm^{-2} (Posthumus *et al.* 1996*a*, *b*). While the laser intensity continues to rise, over-the-barrier ionization occurs each time a next higher appearance intensity is reached. After each ionization process, the kinetic energy of the fragments increases, due to additional Coulomb repulsion. The broken curve in figure 8 traces the classical trajectory for a 150 fs pulse. The ionization steps happen at each first crossing of the broken curve with the solid curves. The figure shows further that the final ionization step occurs at R_c. This trajectory results in two I^{4+} fragments with a total kinetic energy release of 58.8 eV.

Table 1. *Explosion fragment energies*

(Experimental and theoretical kinetic energy releases, in electronvolts, for (Q_1, Q_2) channels of I_2 as a function of laser pulse width (FWHM) in femtoseconds. Experimental data compiled from the measurements of (a) Posthumus *et al.* (1996*b*), (b) Normand (personal communication), (c) Hatherly *et al.* (1990).)

	experiment					theory				
channel	E^{a}_{55}	E^{a}_{100}	E^{b}_{150}	E^{c}_{200}	E^{c}_{400}	E_{55}	E_{100}	E_{150}	E_{200}	E_{400}
(1, 1)	4.9	4.8	4.6	3.7	2.9	5.3	5.3	5.3	5.1	3.9
(1, 2)	9.7	8.9	8.8	7.4	7.3	10.7	10.4	9.1	8.4	7.6
(2, 2)	17.6	16.5	15.6	13.5	12.1	20.9	19.6	15.9	15.4	14.1
(2, 3)	26.0	23.8	24	21	19.5	28.9	26.6	24.2	23.2	21.8
(3, 3)	39.0	35.5	34.8	29.8	16	40	37	34.8	33.9	32.1
(3, 4)	50.3	47.2	46.8	42.3	—	51	47.6	45.2	44.3	—
(4, 4)			60	56.8	16	65.7	61.2	58.8	57.7	35.9
(4, 5)			75.6	72.3	—	80.2	74.8	72.8	70.6	—
(5, 5)			94	88.5	17	97.7	91.9	88.2	74.3	40.1

An equally long pulse at the lower intensity of 8×10^{13} W cm^{-2} leads to the (2,2) channel with an energy release of 15.9 eV. The fate of a molecule depends on its location in the laser focus. At the centre of the focus, molecules are subjected to the highest laser intensities. The highest fragmentation channels therefore originate from the centre of the focus. Lower channels are produced in the outer region of the focus. Consequently, intense pulses of a specific peak intensity produce a whole range of fragmentation channels. Table 1 lists experimental and theoretical kinetic energy releases for various pulse lengths. We note that nearly all values agree to within 5% or 10%. More importantly, the trend of a small decrease in energy with increasing pulse duration is accurately reproduced. We further note that experiment and theory agree on the absence of the (3,4) and (4,5) channels at 400 fs.

The largest discrepancies in table 1 occur for the (3,3), (4,4) and (5,5) channels at 400 fs. With such long pulses (relative to the vibrational period of the molecule), these channels are produced by post-dissociative ionization (PDI), i.e. further ionization of the fragments occurs far beyond R_c. PDI at large R hardly adds any Coulomb energy to the fragments. PDI channels therefore have kinetic energies characteristic of a lower, parent channel. We conclude from the data in table 1 that although the model does not reproduce the exact parent channel, it nevertheless correctly demonstrates the presence of PDI at 400 fs.

(*c*) *Angle-dependent ionization of* I_2

From a theoretical point of view we have thus far assumed that the molecular axis is aligned parallel to the laser E-field. This is a practical starting point for calculations because enhanced ionization is most efficient for this orientation. Also, in order to explain the kinetic energy released in the fragmentation process, it is of little significance whether the natural selection of aligned molecules is enhanced by laser-induced rotation. On the other hand, such dynamic alignment of molecules in intense laser fields is of considerable interest, particularly in the context of coherent control

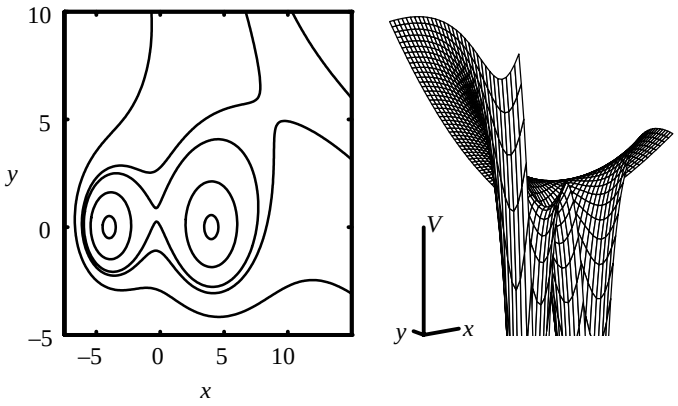

Figure 9. Contour plot and three-dimensional mesh plot of the double potential well in an external E-field at an angle of 45° with the molecular axis. For classical field-ionization the electron must pass across the two saddle points.

(Charron *et al*. 1994). If we wish to study the importance of laser-induced alignment, we must first estimate the purely geometric effect of the angular dependence of ionization probabilities. To this end we calculate the threshold intensities for the ionization of molecules for a range of angles between laser E-field and molecular axis (Posthumus *et al*. 1998*a*). The potential, in the particular case of two ions of equal charge and a homogeneous E-field at 45°, is illustrated in figure 9.

The contours on the left-hand diagram clearly show the location of the saddle points that the electron must traverse in order to escape from the molecule. The 'mesh plot' on the right gives a three-dimensional representation of the potential. The height of the potential at the saddle points is numerically assessed and then compared to the energy level of the outer electron. The energy level is computed in the same way as in the one-dimensional model (Posthumus *et al*. 1996*a*). The maximum Stark shift is now the dot product, $\frac{1}{2}\mathcal{E}\cdot R$. Again, the threshold intensity follows from the minimum E-field required to lower the outer potential barrier below the (raised) energy level. Figure 10 shows the threshold intensities for the escape of an electron from the field of two I^+ ions, as a function of ion separation and for a series of angles between $\mathcal{E}$ and R. At all values of R the threshold intensity rises as the angle increases. This angular dependence is seen to be strongest at R_c, where the thresholds vary by as much as a factor of 5 for orthogonal polarizations.

In general, when a molecule breaks up, it is the laser intensity which pertains when the ions reach R_c that determines the final charge state of the fragments. For example, the threshold intensity for the $I^+ + I^+$ channel at 75° is 3×10^{13} W cm^{-2}, but for molecules that are coincidentally aligned with the laser E-field it is only 10^{13} W cm^{-2}. Thus if I_2 molecules at 0° were subjected to pulses of 3×10^{13} W cm^{-2}, those at the centre of the focus, where the laser intensity is above the threshold of 10^{13} W cm^{-2}, would reach the (1,1) channel. If, however, the molecules are at an angle to the E-field, the threshold rises and the volume inevitably becomes smaller. Molecules at an angle larger than 75° to the E-field cannot reach this channel, not even if they sit at the centre of the focus.

If the molecules are initially randomly orientated and if no laser-induced rotation of the molecular axis takes place, then one would expect that the fragment angu-

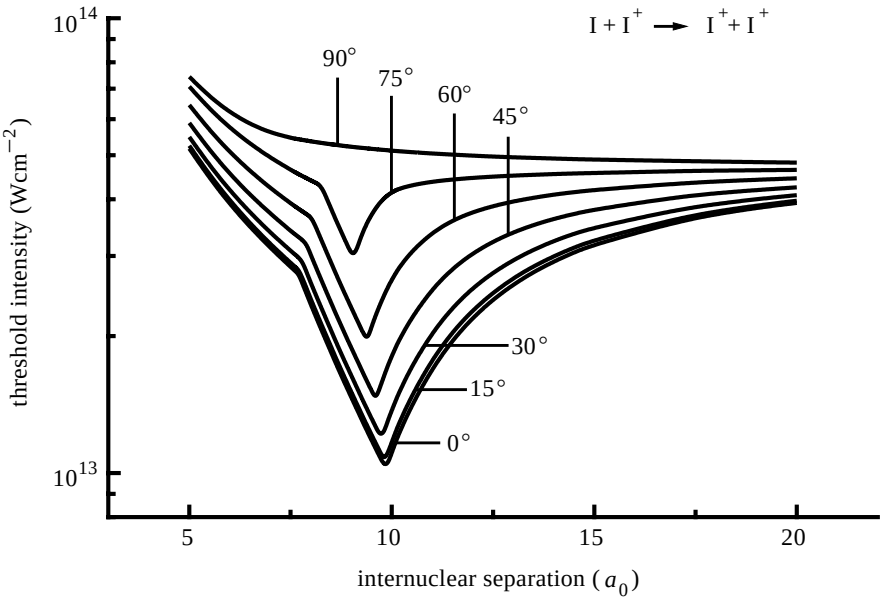

Figure 10. Threshold intensities for the escape of an electron from the field of two I^+ ions, as a function of ion separation and for a series of angles between the laser E-field and the molecular axis.

lar distributions depend critically upon the shell sizes as defined by the threshold intensities. We have calculated the volumes of these shells as a function of angle and show them in figure 11*a* for the (1,2) channel and for a number of laser intensities. Recent experimental results (Posthumus *et al*. 1998*a*) for the angular distributions of this channel are shown in figure 11*b*. Although the agreement with figure 11*a* is by no means perfect, the theoretical and experimental widths (FWHM) are indeed very similar. Furthermore, we note the correspondence in behaviour at 90°. Without dynamic alignment, fragments are bound to appear at 90° when the laser intensity exceeds the threshold at this angle. Given the level of agreement, we conclude that the anisotropy of the I_2 fragments is chiefly due to the angular variation in ionization probabilities rather than any dynamic alignment.

(*d*) *Dynamic alignment of* H_2 *and* N_2

Angular distributions of hydrogen and nitrogen fragment ions were also carefully measured at a range of laser intensities (Posthumus *et al*. 1998*a*). These molecules are lighter than I_2 and therefore more susceptible to reorientation. Perhaps more importantly, due to the higher ionization potentials, these molecules are more resistant to field-ionization and Coulomb explosion and can therefore be subjected to higher E-fields and torques before they dissociate. Figure 12 shows the widths of the $H^+ + H^+$, the $N^+ + N^+$ and the $I^+ + I^{2+}$ angular distributions as a function of laser intensity. Two earlier data points for H_2 (Thompson *et al*. 1997) measured at 750 nm are also included. Below the saturation intensity (where the ionization probability approaches 100%, i.e. 3×10^{14} W cm^{-2} for H_2), the widths of the H_2 and N_2 channels show a small but significant narrowing for higher laser intensities. This is a clear sign of laser-induced dynamic alignment. Also, no matter how much

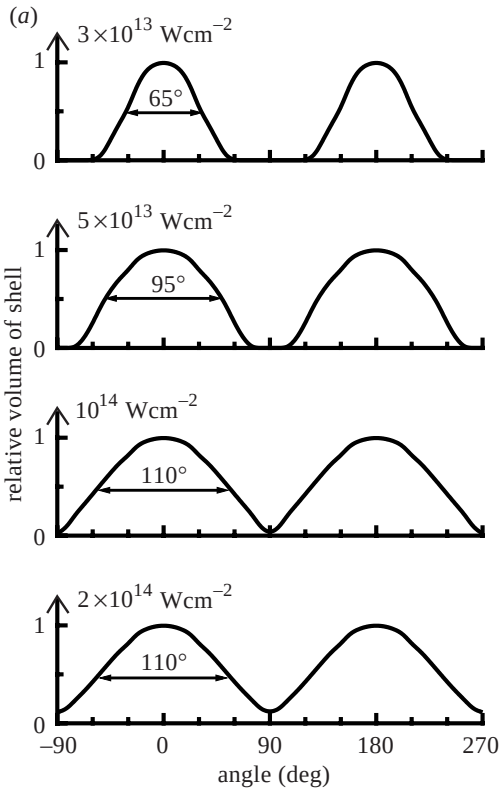

Figure 11. (*a*) The relative volumes of the $I^+ + I^{2+}$ shell, as a function of the angle between the polarization vector and the molecular axis for various laser intensities.

the laser intensity is raised, no fragments are detected at 90°; instead, the angular distributions remain very sharp. The I_2 channel on the other hand has a strikingly different behaviour; it follows quite closely the prediction of the classical model for angle-dependent thresholds.

The modest, counter-intuitive broadening of the $H^+ + H^+$ angular distribution above the saturation intensity can be ascribed to a pulse rise-time effect (Thompson *et al*. 1997): at intensities above saturation, dynamic laser-induced alignment takes place over a shorter interval on the steeper leading edge of the laser pulse. By studying the angular distributions below saturation, this rise-time effect is overcome and the expected sharpening is observed. Considering the data collected thus far, and the results of the present and previous simulations (Thompson *et al*. 1997), we arrive at the following scenario for the multiphoton dissociative ionization of H_2 by intense, 50 fs, Ti:sapphire laser pulses. (1) The molecule starts to be efficiently ionized at an intensity of about 10^{14} W cm^{-2}. (2) The dissociation of H_2^+ follows more or less immediately thereafter (the dissociation threshold of H_2^+ is in fact lower than the ionization threshold of H_2 (Thompson *et al*. 1997). (3) In 10 fs or so, the molecular ion reaches R_c and is ionized to its final state: $H^+ + H^+$. (4) This final state is reached with 100% probability for intensities exceeding 3×10^{14} W cm^{-2}. (5) The H^+ ions are ejected in quite narrow cones around the direction of the laser *E*-field.

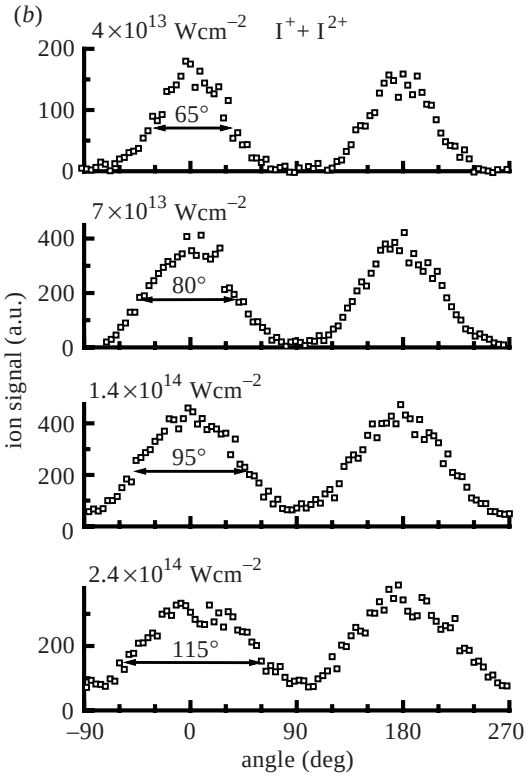

Figure 11. (*Cont.*) (*b*) Angular distributions of the fragments of the $I^+ + I^{2+}$ channel at four laser intensities. The close similarity with the curves in (*a*) indicates that the alignment of the iodine fragments are due to a geometric rather than a dynamic effect.

(*e*) *A spatial pump-probe experiment to test laser-induced alignment*

A double-pulse experiment was performed recently (Posthumus *et al*. 1998*a*) to confirm that within a certain focal volume all H_2 molecules ionize and subsequently fragment in the direction of the laser *E*-field. The experiment employs a Mach–Zehnder-like optical arrangement (figure 13). The first 50 fs pulse to arrive at the focus is linearly polarized with its *E*-field orthogonal to the drift tube axis of the time-of-flight (TOF) analyser. The intensity is approximately 5×10^{14} W cm^{-2}. The H^+ fragments are ejected in the direction perpendicular to the drift tube axis and therefore miss the microchannel plates detector. The second pulse arrives 1 ps later (a very large range of delay times yields the same result). Its *E*-field is along the drift tube axis. Furthermore, the second pulse is focused more sharply, the waist diameter is halved, so as to improve the spatial resolution of this probe pulse. This is achieved by means of a 1:2 beam expander in one of the arms. The energy in the probe pulse is lower, in order to make the focused intensity of the probe about the same as that of the pump.

If the pump and probe are not focused at the same spot, forward and backward H^+ fragment ions created by the probe pulse will be detected. If, on the other hand, the foci spatially overlap, the earlier pump pulse should deplete the focal volume

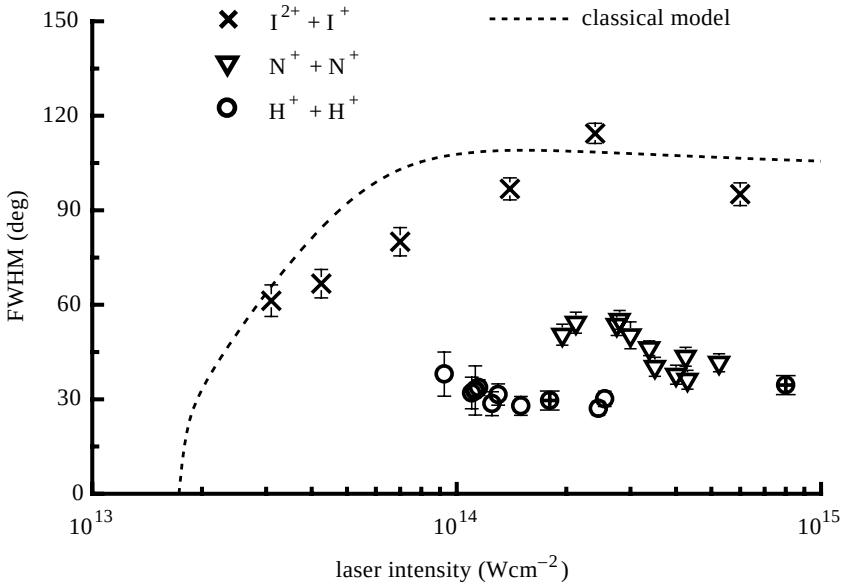

Figure 12. The angular widths of channels of different molecule species as a function of laser intensity. The absence of reorientation of I_2 is clear from the measure of agreement with the model. N_2 and H_2, on the other hand, are forced into alignment. The narrowing with increase in laser intensity provides further evidence of dynamic laser-induced alignment.

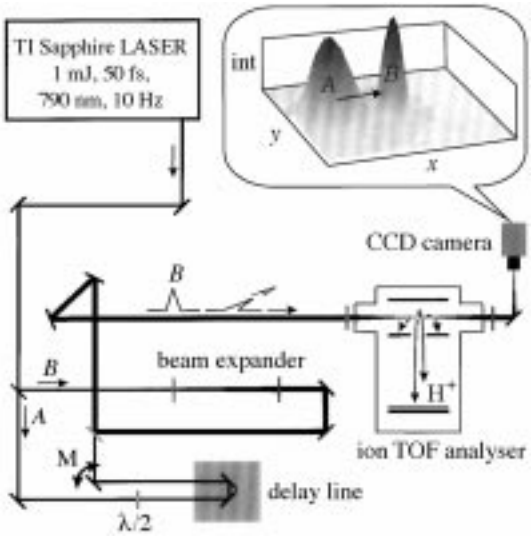

Figure 13. Schematic diagram of the optical arrangement for the pump-probe experiment. The *E*-field of the pump beam is perpendicular to the drift tube axis; the probe's *E*-field is parallel. The inset shows a three-dimensional impression of the two foci as observed on the CCD camera.

of all H_2 (and H_2^+) molecules and thus the probe pulse should be unable to propel H^+ fragments to the detector. In the pump-probe experiment we therefore maintain a constant time delay, but scan the pump beam sideways across the probe. This is

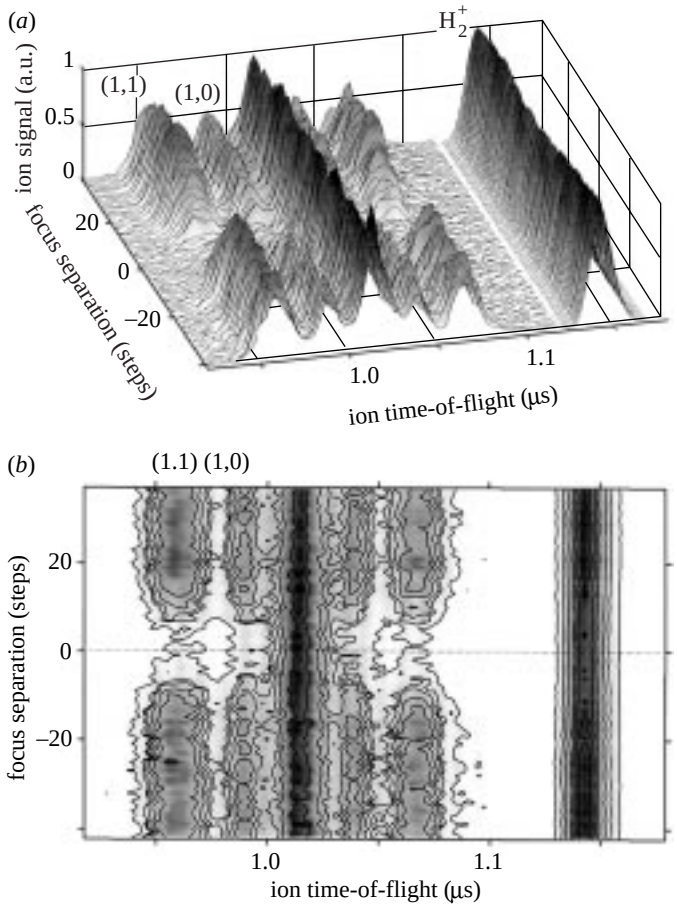

Figure 14. (*a*) H_2 TOF spectra as a function of the spatial separation of the pump and probe foci. When the foci overlap, the fragments disappear completely. (*b*) Contour diagram of the same data as in (*a*).

done by stepwise, electronic adjustment of a mirror (labelled M in figure 13). At each step a TOF spectrum is recorded, averaged over 100 laser shots.

A typical result is shown in figure 14. For clarity, figure 14 shows the same data in different representations. Before discussing the interesting behaviour of the fragments, we first look at the H_2^+ peak at the right of figure 14. These parent ions have no significant kinetic energy and are collected efficiently, irrespective of the polarization of the pulse. We note, nevertheless, that for small separations of the foci, this peak is somewhat lower. The reason is that the total focal volume (pump volume plus probe volume), and therefore the total amount of irradiated molecules, is smaller when the foci overlap.

The TOF spectra show five fragment peaks, two forward and two backward peaks from the probe beam and one central peak from the pump beam. The central peak consists of fragments that, although they are ejected perpendicular to the detector axis, are still collected due to their very low kinetic energy (Hatherley *et al*. 1990). As

expected, the forward and backward fragments produced by the probe beam virtually disappear when the beams overlap. When the same experiment is conducted on I_2, the TOF spectrum is hardly affected; the orthogonal pre-pulse has no significant reorientation effect (Posthumus *et al*. 1998*b*). These results show that the first pulse has indeed ionized and fragmented all H_2 molecules and sent the fragments in the orthogonal direction. The laser must therefore have aligned the molecules parallel to the E-field, since they were originally randomly orientated. Of course, this experiment does not show at what stage the dynamic alignment takes place, but with we suspect that the dissociation and reorientation occur simultaneously.

4. Summary

We have reviewed the theory of multiphoton ionization of molecular ions. Detailed results for H_2^+ were presented for ionization in the multiphoton and tunnelling regimes. We found the quasi-static field ionization model accounts quite successfully for the principal features of the process observed in experiments. Indeed this approach, by virtue of its simplicity and ease of calculation, earns our recommendation even for processes in the region $\gamma \sim 1$. The use of two-colour ultrashort pulses was also reviewed. A classical approach, the FICE model describes the enhanced ionization process at the critical internuclear distance, R_c, in simple terms. Furthermore, it quite accurately reproduces the kinetic energy releases and threshold intensities of the various fragmentation channels of I_2. With the three-dimensional FICE model, threshold intensities as a function of angle between the molecular axis and the laser E-field are calculated. Since the thresholds are low for molecules parallel to the E-field, an angular distribution of fragments arises that is peaked along the polarization axis. We find that the calculated angular distributions, involving only the angle-dependent variation in thresholds, are very similar to the measured angular distributions of the I_2 fragments. Conversely, the lighter molecules (H_2 and N_2) are reorientated by the laser field. The difference in behaviour of the H_2 and I_2 molecules is further highlighted by a new pump-probe experiment.

We acknowledge the UK Engineering and Physical Sciences Research Council for their financial support of this work. We also thank Dr Martin Plummer and Professor Keith Codling for very useful discussions.

References

Baik, M.-G., Pont, M. & Shakeshaft, R. 1996 *Phys. Rev.* A **54**, 1570.
Charron, E., Giusti-Suzor, A. & Mies, F. H. 1994 *Phys. Rev.* A **49**, R641.
Chelkowski, S., Zuo, T., Atabek, O. & Bandrauk, A. D. 1995 *Phys. Rev.* A **52**, 2977.
Codling, K. & Frasinski, L. J. 1993 *J. Phys.* B **26**, 783.
Giusti-Suzor, A., Mies, F. H., DiMauro, L. F., Charron, E. & Yang, B. 1995 *J. Phys.* B **28**, 309.
Hatherly, P. A., Frasinski, L. J. & Codling, K. 1990 *J. Phys. Lett.* B **23**, 291.
Keldysh, L. V. 1965 *Sov. Phys. JETP* **20**, 1307.
Kulander, K. C., Mies, F. H. & Schafer, K. J. 1996 *Phys. Rev.* A **53**, 2562.
Madsen, L. B. & Plummer, M. 1998 *J. Phys.* B **31**, 87.
Maquet, A., Chu, S.-I. & Reinhardt, W. P. 1983 *Phys. Rev.* A **27**, 2946.
Plummer, M. & McCann, J. F. 1995*a* *J. Phys.* B **28**, 4073.
Plummer, M. & McCann, J. F. 1995*b* *J. Phys. Lett.* B **28**, 119.

Plummer, M. & McCann, J. F. 1996 *J. Phys.* B **29**, 4625.

Plummer, M. & McCann, J. F. 1997 *J. Phys. Lett.* B **30**, 401.

Posthumus, J. H., Frasinski, L. J., Giles, A. J. & Codling, K. 1995 *J. Phys. Lett.* B **28**, 349.

Posthumus, J. H., Giles, A. J., Thompson, M. R., Shaikh, W., Langley, A. J., Frasinski, L. J. & Codling, K. 1996*a* *J. Phys. Lett.* B **29**, 525.

Posthumus, J. H., Giles, A. J., Thompson, M. R. & Codling, K. 1996*b* *J. Phys.* B **29**, 5811.

Posthumus, J. H., Plumridge, J., Thomas, M. H., Codling, K., Frasinski, L. J., Langley, A. J. & Taday, P. F. 1998*a* *J. Phys. Lett.* B **31**, 553–562.

Posthumus, J. H., Plumridge, J., Frasinski, L. J., Codling, K., Langley, A. J. & Taday, P. F. 1998*b* *J. Phys.* B **31**, 985–993.

Potvliege, R. M. & Shakeshaft, R. 1992 *Adv. At. Mol. Phys.* (Suppl. I), p. 373.

Sanderson, J. H., Thomas, R. V., Bryan, W. A., Newell, W. R., Taday, P. F. & Langley, A. J. 1997 *J. Phys.* B **30**, 4499.

Sanderson, J. H., Thomas, R. V., Bryan, W. A., Newell, W. R., Langley, A. J. & Taday, P. F. 1998 *J. Phys. Lett.* B **31**, 599.

Seideman, T., Ivanov, M. Yu. & Corkum, P. B. 1995 *Phys. Rev. Lett.* **75**, 2819.

Shao, Y. L., Ditmire, T., Tisch, J. W. G., Springate, E., Marangos, J. P. & Hutchinson, M. R. 1996 *Phys. Rev. Lett.* **77**, 3343.

Thompson, M. R., Thomas, M. K., Taday, P. F., Posthumus, J. H., Langley, A. J., Frasinski, L. J. & Codling, K. 1997 *J. Phys.* B **30**, 5755.

van Linden van den Heuvel, H. B. & Muller, H. G. 1988 *Multiphoton processes* (ed. S. J. Smith & P. L. Knight). Cambridge University Press.

Walker, B., Sheehy, B., DiMauro, L. F., Agostini, P., Shafer, K. J. & Kulander, K. C. 1994 *Phys. Rev. Lett.* **73**, 1277.

Zuo, T. & Bandrauk, A. D. 1995 *Phys. Rev.* A **52**, R2511.

PHILOSOPHICAL TRANSACTIONS OF THE ROYAL SOCIETY A MATHEMATICAL, PHYSICAL & ENGINEERING SCIENCES